

An equation-of-state-insensitive measure of neutron star stiffness

Jayana Saes* and Raissa F. P. Mendes†

Instituto de Física, Universidade Federal Fluminense, Niterói, Rio de Janeiro, 24210-346, Brazil.

(Dated: September 27, 2021)

Universal relations (i.e., insensitive to the equation of state) between macroscopic properties of neutron stars (NSs) have proven useful for a variety of applications—from providing a direct means to extract observables from data to breaking degeneracies that hinder tests of general relativity. Similarly, equation-of-state insensitive relations directly connecting macroscopic and microscopic properties of NSs can potentially provide a clean window into the behavior of nuclear matter. In this Letter, we uncover a tight correlation between certain macroscopic properties of NSs—its compactness, moment of inertia or tidal deformability—and the ratio of central pressure to central energy density, which can be interpreted as a mean notion of the stiffness of nuclear matter inside a NS. We describe interesting properties of this stiffness measure, quantify its universality, and explore its consequences in the face of recent NS observations.

Introduction.—Different observational channels are nowadays converging to compose an increasingly clear picture of neutron stars (NSs). Radio observations of rotation-powered pulsars have enabled accurate mass measurements for the components of a number of binary systems (see, e.g. [1–3]), while pulse profile modeling of the X-ray data from the Neutron-Star-Interior-Composition Explorer (NICER) already provided measurements of the radius of two NSs [4–7], improving the accuracy of previous radii estimates. Additionally, observation of gravitational waves (GWs) from the binary NS merger GW170817 allowed a first measurement of the tidal deformability [8, 9], with its electromagnetic counterpart providing valuable information about the remnant [10]. Future years should witness the measurement of additional NS properties, such as their moment of inertia [11] or characteristic pulsation modes [12–14].

All of these observables depend on the nuclear equation of state (EOS), which, for a cold NS, consists of a one-parameter relation between pressure and rest-mass density, $p = p(\rho)$. At the supra-nuclear densities thought to exist in NS cores, the EOS is mostly unconstrained by nuclear physics experiments. As a result, different theoretical strategies to extrapolate nuclear physics models to this high density regime give rise to disparate predictions for NS properties [15, 16].

Interestingly, EOS-insensitive relations have been found to exist between several macroscopic NS observables (see e.g. [17] and references therein). These relations are particularly useful to break degeneracies that would otherwise hinder an accurate estimation of NS properties. For example, the “binary Love relation” [18, 19] between certain combinations of the tidal deformabilities of the components of a binary system can be used to infer the individual deformabilities, which are not currently measurable in GW data. Moreover, EOS-insensitive relations make comparison between various

measurements of NS properties more straightforward. For instance, one can use the Love- C [20, 21] relation, between the tidal deformability and the NS compactness, to translate a measurement of mass and tidal deformability— inferred from GW data—into an estimate of the NS radius, making comparison with other radius measurements (say, from NICER data) more direct. Some EOS-insensitive relations, such as those connecting moment of inertia, tidal deformability and quadrupole moment (“I-Love-Q”) are incredibly tight, holding to roughly percent accuracy [20].

EOS-insensitive relations have also been found, relating directly macroscopic and microscopic observables. For instance, pressure at \sim 1-2 times the nuclear saturation density ($\rho_s = 2.8 \times 10^{14} \text{ g cm}^{-3}$) was found to correlate to the radius of a typical NS [22], while pressure at higher densities ($\sim 7\text{-}8 \rho_s$) is thought to determine their maximum mass [23]. Estimates for the pressure at fiducial densities, coming from NS observations, can then be fed into nuclear physics models, constraining properties of the nuclear interaction such as the nuclear symmetry energy [24, 25].

The aim of this work is to explore a new EOS-insensitive relation between certain macroscopic NS properties and a microscopic measure of the mean stiffness of nuclear matter inside a NS, namely, the ratio $\alpha_c \equiv p_c/\epsilon_c$ of central pressure to central energy density. This stiffness measure harbors similarities with more commonly used notions, such as the maximum speed of sound inside a NS. However, it correlates much more strongly with macroscopic observables such as the NS compactness (C), dimensionless moment of inertia (\tilde{I}) or tidal deformability ($\tilde{\Lambda}$). The approximate universal $\alpha_c - C$, $\alpha_c - \tilde{I}$, and $\alpha_c - \tilde{\Lambda}$ relations are analyzed in this work both for a restricted set of realistic EOS and for a larger set of $\sim 15,000$ phenomenological EOS (see Figs. 1 and 2). As an example, the $\alpha_c - \tilde{\Lambda}$ relation is found to hold to a maximum error of $\sim 7\%$ for the set of realistic EOS, and to a maximum error of $\sim 30\%$ for the set of phenomenological EOS, with 90% of the error below $\sim 8\%$. Measurements of tidal deformability, moment of inertia or compactness can thus be translated

* jayanasae@id.uff.br

† rfpmendes@id.uff.br

into estimates for α_c , providing direct information about the behavior—and extremeness—of nuclear matter inside NSs.

Properties of the stiffness measure.— The stiffness of nuclear matter encodes how pressure increases as density increases. Commonly used measures include the adiabatic sound speed¹,

$$c_s = \sqrt{\left. \frac{\partial p}{\partial \epsilon} \right|_s} \quad (1)$$

and the adiabatic index

$$\Gamma_1 = \left(\frac{\partial \ln p}{\partial \ln \rho} \right)_s, \quad (2)$$

where ϵ and s are the fluid total energy density and entropy as measured by comoving observers. Both (1) and (2) are local stiffness measures: For each value of the energy density, $c_s^2(\epsilon)$ measures the slope of the $p(\epsilon)$ relation, and similarly for Γ_1 . On the other hand, one can think of the ratio

$$\alpha(\epsilon) \equiv \frac{p(\epsilon)}{\epsilon} \quad (3)$$

as a global, or mean, notion of the stiffness of nuclear matter up to a certain value of the energy density.

Similarly to the sound speed, the ratio p/ϵ is deeply connected to the principle of causality, which requires that the velocity of causal influences should not exceed the speed of light. For a perfect fluid, with energy-momentum tensor

$$T^{\mu\nu} = (\epsilon + p)u^\mu u^\nu + pg^{\mu\nu}, \quad (4)$$

where u^μ is the four-velocity of fluid elements, the sound speed (1) determines the propagation speed of sound waves, and causality then implies that [28]

$$c_s \leq 1. \quad (5)$$

On the other hand, the dominant energy condition (DEC)—which is the statement that the current of energy-momentum density, $-T_{\nu}^{\mu}\xi^{\nu}$, as measured by observers with four-velocity ξ^{μ} , should be future-directed or null—implies, for a perfect fluid (4), that $\epsilon \geq |p|$, or

$$\alpha \leq 1 \quad (6)$$

if $p \geq 0$. For a fluid characterized by a conserved energy-momentum tensor, the DEC implies that matter cannot travel faster than light, as it can be shown that if $T^{\mu\nu}$ vanishes on a close, achronal set S , it also vanishes in the domain of dependence of S (see lemma 4.3.1 in [29]). Therefore, condition (6) is also a statement about causal behavior of the fluid².

Of course, since in the nonrelativistic limit nuclear matter satisfies $p \ll \epsilon \approx \rho$, for the bound $\alpha = 1$ to be achieved, the fluid must first go superluminal; Eq. (5) is therefore more restrictive than (6). In particular, it is interesting to consider the case of an EOS that is “maximally soft”, $p(\epsilon) = 0$, for $\epsilon \leq \epsilon_0$, and “maximally stiff”, $p(\epsilon) = \epsilon - \epsilon_0$, for $\epsilon \geq \epsilon_0$, which yields the most compact NS models [32]. The maximally compact configuration, with $C \approx 0.35$, has $\epsilon_c = 3.024\epsilon_0$ and $p_c = 2.034\epsilon_c$ (with the subscript c denoting the stellar center) and therefore

$$\alpha_c = 0.670. \quad (7)$$

As we will see below, by requiring that the EOS satisfies Eq. (5), the bound (7) is approached, rather than (6).

Another relevant value for the stiffness measure (3) is $\alpha = 1/3$. Since $T \equiv g_{\mu\nu}T^{\mu\nu} = (3\alpha - 1)\epsilon$ for a perfect fluid, $\alpha = 1/3$ corresponds to $T = 0$. Again, for the value $\alpha = 1/3$ to be reached inside a NS, the conformal bound $c_s^2 < 1/3$ [33] must necessarily be violated in its interior. Notably, it has been pointed out before that the stellar compactness at which $T = 0$ at the stellar center is roughly EOS-independent [34]. This can be seen as a particular case of the more general, EOS-insensitive relation between the NS compactness and any specific value of α_c , which we now discuss.

Approximate universality.—Here we explore the relation between the stiffness measure $\alpha_c = p_c/\epsilon_c$ and the NS compactness, moment of inertia and tidal deformability, for different choices of realistic or phenomenological EOS. The NS compactness, $C = M/R$, is computed from its mass M and radius R , obtained by numerically solving the TOV equations for spherically symmetric hydrostatic equilibrium. The NS moment of inertia, $I = J/\Omega$, is computed from its angular momentum J and angular velocity Ω in the approximation of slow rotation [35]. From it we construct the dimensionless quantity $\bar{I} = I/M^3$, which is known to obey an EOS-insensitive relation with C [36]. Finally, the tidal deformability is computed by considering quadrupolar perturbations to an isolated NS; it measures the strength of the quadrupole moment Q_{ij} induced in a NS by an external tidal field \mathcal{E}_{ij} : $Q_{ij} = -\Lambda \mathcal{E}_{ij}$ [37–39]. Again, we consider its dimensionless version, $\tilde{\Lambda} = \Lambda/M^5$, which is also known to obey an EOS-insensitive relation with C [21].

In order to explore the relation between α_c and the macroscopic observables C , \bar{I} , and $\tilde{\Lambda}$, we first consider a set of 25 realistic equations of state (see Appendix A of Ref. [40] for details), in the generalized piecewise polytropic (GPP) approximation discussed in Ref. [41]. Results are shown in Fig. 1. We consider sixth order polynomial fits of the form

$$\ln \alpha_c = \sum_{j=0}^6 a_j O^j, \quad (8)$$

where $O \in \{C, \ln \bar{I}, \ln \tilde{\Lambda}\}$, with coefficients a_j given in Table I. For low compactness ($C \lesssim 0.2$), the $\alpha_c - C$ relation holds

¹ We adopt natural units, $c = G = 1$, unless stated otherwise.

² Note that it is in principle possible to construct special Lorentz invariant (causal) theories that violate both Eqs. (5) and (6) [30, 31].

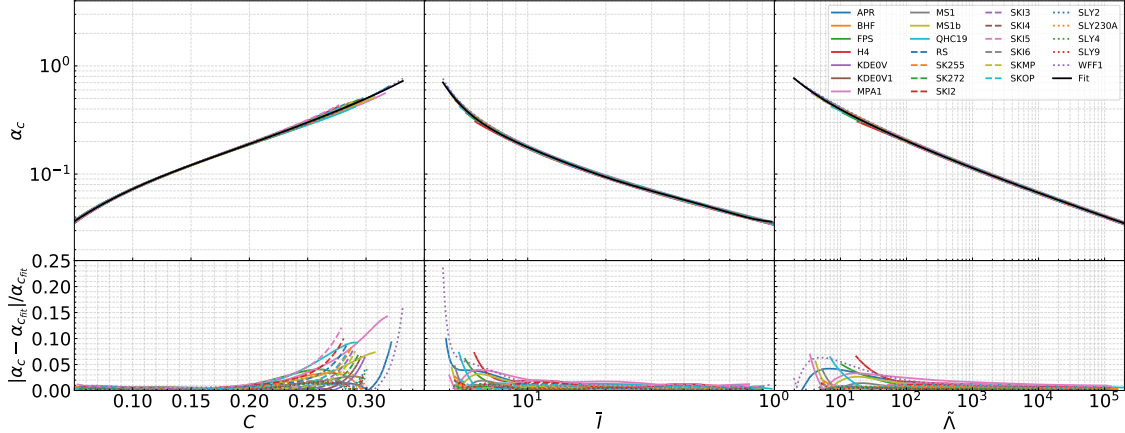


Figure 1: Universal $\alpha_c - C$, $\alpha_c - I$ and $\alpha_c - \tilde{\Lambda}$ relations for a set of 25 realistic EOS. A black line represents a sixth order polynomial fit (as in Eqs. 8), and bottom panels display the corresponding relative error. Only configurations with $C > 0.05$ are considered.

EOS	Relation	a_0	a_1	a_2	a_3	a_4	a_5	a_6
Realistic	$\alpha_c - C$	-4.265	21.78	-43.05	-3.053×10^2	2.696×10^3	-7.397×10^3	7.260×10^3
	$\alpha_c - I$	54.22	-108.62	89.47	-39.38	9.653	-1.246	6.614×10^{-2}
	$\alpha_c - \tilde{\Lambda}$	0.1336	-0.6549	0.1246	-2.196×10^{-2}	2.259×10^{-3}	-1.224×10^{-4}	2.696×10^{-6}
Phenomenological	$\alpha_c - C$	-4.538	29.83	-1.517×10^2	4.223×10^2	4.214×10^2	-4.452×10^3	6.098×10^3
	$\alpha_c - I$	35.82	-67.80	52.72	-22.19	5.236	-0.6540	3.372×10^{-2}
	$\alpha_c - \tilde{\Lambda}$	-0.1305	-0.3646	-3.770×10^{-3}	5.541×10^{-3}	-8.364×10^{-4}	5.377×10^{-5}	-1.304×10^{-6}

Table I: Fit coefficients to the $\alpha_c - C$, $\alpha_c - I$ and $\alpha_c - \tilde{\Lambda}$ relations, for a set of 25 realistic EOS (upper rows), and a set of 15,000 phenomenological EOS (lower rows).

to a relative error of less than 2%, but the error increases for higher values of C , up to a maximum of $\sim 16\%$. Similarly, the universality of the $\alpha_c - I$ and $\alpha_c - \tilde{\Lambda}$ relations is stronger for larger values of I and $\tilde{\Lambda}$, and slightly weaker for lower values: The $\alpha_c - I$ relation holds to a maximum error of $\sim 24\%$, while the $\alpha_c - \tilde{\Lambda}$ relation holds to a maximum error of $\sim 7\%$ for this set of realistic EOS. Note that the bound (7) is violated by the WFF1 EOS, but only because this EOS becomes acausal below the central density of the maximum mass configuration.

In order to further probe the universality of these relations, we explore a larger set of phenomenological EOS. We adopt the GPP parametrization developed in Ref. [41], in which one defines density intervals $\rho_0 < \rho_1 < \rho_2 < \dots$ above a certain value ρ_0 , in such a way that

$$p(\rho) = K_i \rho^{\Gamma_i} + \Lambda_i, \quad \rho_{i-1} \leq \rho \leq \rho_i. \quad (9)$$

The energy density $\epsilon(\rho)$ can be obtained from (9) and the first law of thermodynamics. This generalizes the usual piecewise polytropic parametrization (see, e.g. Ref. [42]) by introducing the parameters Λ_i , which can be adjusted in order to guarantee that the speed of sound (1) is everywhere continuous. One

disadvantage of this construction is that Γ_i does not coincide with the adiabatic index (2) in each polytropic phase, rendering its interpretation less natural. Following Ref. [41], we fix the crust to the SLy(4) EOS, and divide the core into three density intervals, with dividing densities $\rho_1 = 10^{14.87} \text{ g/cm}^3$ and $\rho_2 = 10^{14.99} \text{ g/cm}^3$. Four free parameters define the EOS, which can be taken as K_1 and Γ_i , $i \in \{1, 2, 3\}$, while the remaining ones are determined by continuity and differentiability requirements.

We generate $\sim 15,000$ phenomenological EOS by randomly sampling GPP parameters in the ranges $\Gamma_i \in [-2.0, 8.0]$. For each value of Γ_1 , $\log K_1$ is randomly sampled in the interval $[\log K_{\min}(\Gamma_1), \log K_{\max}(\Gamma_1)]$, where K_{\max} is determined by the requirement that the density ρ_{div} that divides crust and core satisfies $\rho_{\text{div}} < \rho_1$, and K_{\min} is determined by requiring that $\rho_{\text{div}} > \rho_{\text{crust,min}}$, where $\rho_{\text{crust,min}} = 5.317 \times 10^{11} \text{ g/cm}^3$ is the last dividing density for a GPP parametrization of the crust (see Table II of Ref. [41]). For $\Gamma_1 \lesssim 1.38$, we have that $K_{\min} > K_{\max}$; therefore the parameters do not generate a consistent GPP model. In practice, then, $\Gamma_1 \gtrsim 1.38$. We further require that all accepted EOS (i) allow a maximum

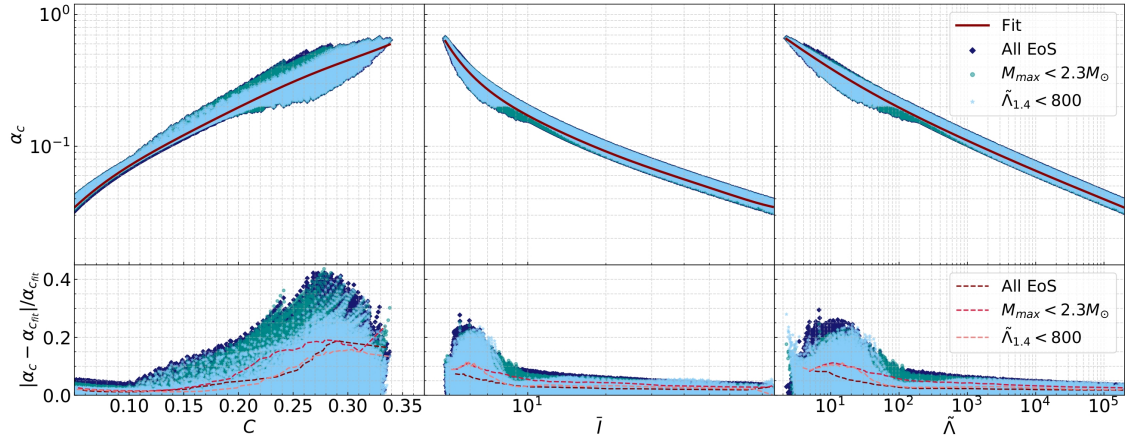


Figure 2: Universal $\alpha_c - C$, $\alpha_c - \bar{I}$ and $\alpha_c - \tilde{\Lambda}$ relations for a set of $\sim 15,000$ phenomenological EOS. Data for the full set of EOS is shown in dark-blue, while those obeying the additional requirement that the dimensionless tidal deformability of a $1.4M_\odot$ NS is $\tilde{\Lambda}_{1.4M_\odot} < 800$ are shown in light blue, and those with a maximum mass $M_\odot < 2.3M_\odot$ are shown in cyan. A red line represents a sixth order polynomial fit (as in Eq. 8) to the full set of EOS. Bottom panels display the corresponding relative error, with lines enclosing 90% of the errors. Only configurations with $C > 0.05$ are displayed.

NS mass of at least $2.0M_\odot$, and (ii) are causal, in the sense that Eq. (5) holds for all hydrodynamically stable configurations. We also explore the effect of imposing the additional requirements that either (iii) $\tilde{\Lambda}_{1.4M_\odot} < 800$, corresponding to the 90% credible upper bound for the tidal deformability of a $1.4M_\odot$ NS derived from the GW event GW170817 [8], or (iv) $M_{\max} < 2.3M_\odot$, which is a reasonable condition for the maximum mass coming from analysis of GW170817 and its electromagnetic counterpart [43–45]. As we will see, the approximate universal relations are not strongly influenced by these additional requirements. For each accepted EOS, we generate 50 equilibrium configurations with central densities between $\rho_{\text{crust,min}}$ and that corresponding to the solution with maximum mass (ρ_{\max}). In all plots, we only display configurations with $C > 0.05$.

Figure 2 shows the $\alpha_c - C$, $\alpha_c - \bar{I}$, and $\alpha_c - \tilde{\Lambda}$ relations for our set of 15,000 phenomenological EOS, together with fits of the form (8) and the corresponding residuals. For this set of EOS, the $\alpha_c - C$ relation holds to a maximum error of $\sim 42\%$, with 90% of errors below $\sim 7\%$; the $\alpha_c - \bar{I}$ relation holds to a maximum error of $\sim 28\%$, with 90% of the errors below $\sim 7\%$; and the $\alpha_c - \tilde{\Lambda}$ relation holds to a maximum error of $\sim 29\%$, with 90% of errors below 8%. The maximum value of α_c generated in this set of equilibrium solutions is ~ 0.662 , lower than the bound (7), which is expected since only EOS with subluminal sound speeds are included in this set. It is worthwhile to mention that roughly 10% of the EOS in our set display an important softening at high densities, in such a way that $\alpha(\rho)$ is not a monotonically increasing function of ρ up to the central density of the most massive configuration.

These EOS contribute significantly to the larger spread seen in Fig. 2 for high values of C (or low \bar{I} , $\tilde{\Lambda}$). We also emphasize that although α shares some properties with the speed of sound, the correlation that is seen between α_c and C , \bar{I} or $\tilde{\Lambda}$ is much weaker for, say, the sound speed at $r = 0$, $c_{s,c}$. This is illustrated in Fig. 3, where the $\alpha_c - \tilde{\Lambda}$ and $c_{s,c}^2 - \tilde{\Lambda}$ relations are shown.

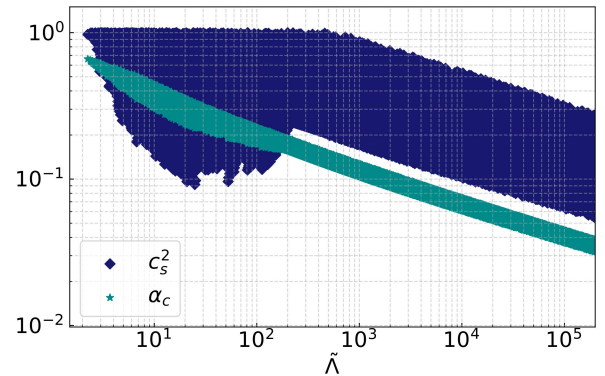


Figure 3: The ratio $\alpha_c = p_c/\epsilon_c$ and the square of the speed of sound at the stellar center, $c_{s,c}^2$, are shown as a function of $\tilde{\Lambda}$ for a collection of equilibrium configurations obeying a set of $\sim 15,000$ phenomenological EOS.

Connecting to observations.—We proceed to explore connections to recent observations by determining the posterior distribution for α_c for three NSs: The primary and secondary components of the GW event GW170817, for which masses

and tidal deformabilities have been measured [9], and pulsar J0740+6620, for which mass and radius have been measured [6, 7]. Although NICER observations of pulsar J0030+0451 have also enabled estimates of its mass and radius [4, 5], we do not consider this NS in our analysis, since its $\sim 1.4M_{\odot}$ mass falls in the same range as the binary components that originated GW170817.

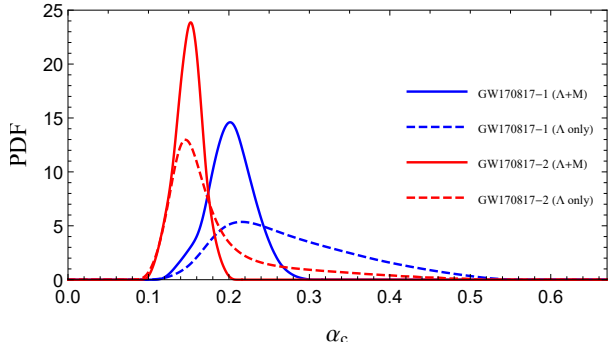


Figure 4: Posterior PDF for α_c for the primary (1, in blue) and secondary (2, in red) components of the GW170817 event. For the dashed curves, only the tidal deformability was taken into account, while solid curves also include information about the measured masses.

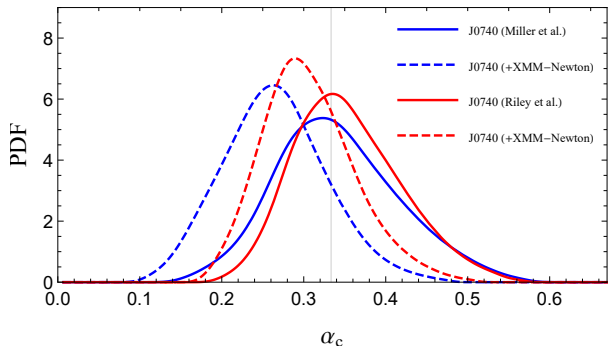


Figure 5: Posterior PDF for α_c for the massive pulsar J0740+6620, taking into account its mass and radius measurements, from the analyzes of Ref. [6] (blue curves) and [7] (red curves). Solid curves were obtained from data that used NICER measurements alone, while dashed curves also include spectroscopic data from XMM-Newton. A vertical line highlights the value $\alpha_c = 1/3$.

In each case we compute $p(\alpha_c|\vec{D}, I)$, the posterior probability for α_c given some measurement of NS properties \vec{D} and background information I , by marginalizing $p(\alpha_c, \vec{\theta}|\vec{D}, I)$ over EOS parameters $\vec{\theta} = \{\log K_1, \Gamma_1, \Gamma_2, \Gamma_3\}$. The probability $p(\alpha_c, \vec{\theta}|\vec{D}, I)$ that a star with properties \vec{D} has a given value α_c of central pressure to central energy density and EOS parameters $\vec{\theta}$ is computed from Bayes theorem,

$$p(\alpha_c, \vec{\theta}|\vec{D}, I) = \mathcal{N}p(\vec{D}|\alpha_c, \vec{\theta}, I)p(\alpha_c, \vec{\theta}|I), \quad (10)$$

where \mathcal{N} is a normalization factor. The prior $p(\alpha_c, \vec{\theta}|I)$ can be factored as $p(\alpha_c, \vec{\theta}|I) = p(\alpha_c|\vec{\theta}, I)p(\vec{\theta}|I)$. We assume the EOS prior $p(\vec{\theta}|I)$ to be uniform in the ranges discussed previously, and $p(\alpha_c|\vec{\theta}, I)$ to be uniform in the range $\alpha(\rho_{\text{crust,min}}) \leq \alpha_c \leq \alpha(\rho_{\text{max}})$, where ρ_{max} is the central density for the most massive NS predicted by an EOS with parameters $\vec{\theta}$. The likelihood $p(\vec{D}|\alpha_c, \vec{\theta}, I)$ is inferred from publicly available experimental distributions [6, 7, 9]. In computing this likelihood, one has to take into account the fact $\alpha(\rho)$ may not be a monotonically increasing function of ρ in the range of interest, so that the inverse relation may not be single-valued.

Figure 4 shows the posterior probability density function (PDF) for α_c for the primary (1) and secondary (2) components of the binary NS system that originated GW170817. Dashed lines show the PDF obtained by only taking into account the measurement of the tidal deformabilities. The spread in the PDF reflects the uncertainty in the measurement of $\tilde{\Lambda}_{1,2}$, specially for the primary, more massive, component. Narrower PDFs are obtained by including the components' mass measurements (solid lines). We obtain a median and 90% credible interval of $\alpha_c = 0.202^{+0.05}_{-0.05}$ for the primary and $\alpha_c = 0.151^{+0.03}_{-0.03}$ for the secondary component.

Perhaps more interesting from the point of view of probing extreme properties of nuclear matter is the case of the massive pulsar J0740+6620, with mass $2.08 \pm 0.07M_{\odot}$ (68.3% credibility) [27], which recently had its radius measured. In Fig. 5 we show the posterior PDF for α_c , by taking into account mass and radius measurements for J0740+6620 as analyzed in Refs. [6, 7]. Using data from Riley et al., for instance, we obtain a median and 90% credible interval of $\alpha_c = 0.348^{+0.126}_{-0.093}$ when the likelihood is derived from NICER data alone, and of $\alpha_c = 0.301^{+0.107}_{-0.082}$ when XMM-Newton data is included. The last median agrees well with the value we get, of ≈ 0.300 , by using the universal $\alpha_c - C$ relation with coefficients given in Table I and $C \approx 0.247$ [7]. It is interesting to note that all distributions have a significant support in the region $\alpha_c > 1/3$, which corresponds to a positive value of the trace of the energy-momentum tensor in the stellar center. For the values reported by Riley et al., the probability that $\alpha_c > 1/3$ is $\sim 61\%$ for NICER-only data, and $\sim 31\%$ when XMM-Newton data is included in the analysis. With the increase in accuracy of NS observations, one should be able to infer precisely the value of α_c through the approximately universal relations uncovered in this work, providing a clear window into the extremeness of nuclear matter inside NSs.

ACKNOWLEDGMENTS

This work was partially supported by the National Council for Scientific and Technological Development (CNPq), and by the Carlos Chagas Filho Research Support Foundation (FAPERJ).

[1] M. Kramer, I. H. Stairs, R. N. Manchester, M. A. McLaughlin, A. G. Lyne, R. D. Ferdman, M. Burgay, D. R. Lorimer, A. Possenti, N. D'Amico, J. M. Sarkissian, G. B. Hobbs, J. E. Reynolds, P. C. C. Freire, and F. Camilo, *Science* **314**, 97 (2006).

[2] J. M. Weisberg, D. J. Nice, and J. H. Taylor, *The Astrophysical Journal* **722**, 1030 (2010).

[3] E. Fonseca, I. H. Stairs, and S. E. Thorsett, *The Astrophysical Journal* **787**, 82 (2014).

[4] M. C. Miller, F. K. Lamb, A. J. Dittmann, S. Bogdanov, Z. Arzoumanian, K. C. Gendreau, S. Guillot, A. K. Harding, W. C. G. Ho, J. M. Lattimer, R. M. Ludlam, S. Mahmoodifar, S. M. Morsink, P. S. Ray, T. E. Strohmayer, K. S. Wood, T. Enoto, R. Foster, T. Okajima, G. Prigozhin, and Y. Soong, *The Astrophysical Journal* **887**, L24 (2019).

[5] T. E. Riley, A. L. Watts, S. Bogdanov, P. S. Ray, R. M. Ludlam, S. Guillot, Z. Arzoumanian, C. L. Baker, A. V. Bilous, D. Chakrabarty, K. C. Gendreau, A. K. Harding, W. C. G. Ho, J. M. Lattimer, S. M. Morsink, and T. E. Strohmayer, *The Astrophysical Journal* **887**, L21 (2019).

[6] M. C. Miller, F. K. Lamb, A. J. Dittmann, S. Bogdanov, Z. Arzoumanian, K. C. Gendreau, S. Guillot, W. C. G. Ho, J. M. Lattimer, M. Loewenstein, S. M. Morsink, P. S. Ray, M. T. Wolff, C. L. Baker, T. Cazeau, S. Manthripragada, C. B. Markwardt, T. Okajima, S. Pollard, I. Cognard, H. T. Cromartie, E. Fonseca, L. Guillemot, M. Kerr, A. Parthasarathy, T. T. Pennucci, S. Ransom, and I. Stairs, “The radius of psr j0740+6620 from nicer and xmm-newton data,” (2021), arXiv:2105.06979 [astro-ph.HE].

[7] T. E. Riley, A. L. Watts, P. S. Ray, S. Bogdanov, S. Guillot, S. M. Morsink, A. V. Bilous, Z. Arzoumanian, D. Choudhury, J. S. Deneva, K. C. Gendreau, A. K. Harding, W. C. G. Ho, J. M. Lattimer, M. Loewenstein, R. M. Ludlam, C. B. Markwardt, T. Okajima, C. Prescod-Weinstein, R. A. Remillard, M. T. Wolff, E. Fonseca, H. T. Cromartie, M. Kerr, T. T. Pennucci, A. Parthasarathy, S. Ransom, I. Stairs, L. Guillemot, and I. Cognard, “A nicer view of the massive pulsar psr j0740+6620 informed by radio timing and xmm-newton spectroscopy,” (2021), arXiv:2105.06980 [astro-ph.HE].

[8] B. P. Abbott, R. Abbott, T. D. Abbott, *et al.* (LIGO Scientific Collaboration and Virgo Collaboration), *Phys. Rev. Lett.* **119**, 161101 (2017).

[9] B. P. Abbott, R. Abbott, T. D. Abbott, *et al.* (The LIGO Scientific Collaboration and the Virgo Collaboration), *Phys. Rev. Lett.* **121**, 161101 (2018).

[10] B. P. Abbott, R. Abbott, T. D. Abbott, *et al.*, *The Astrophysical Journal* **848**, L12 (2017).

[11] M. Kramer and N. Wex, *Classical and Quantum Gravity* **26**, 073001 (2009).

[12] J. Clark, A. Bauswein, L. Cadonati, H.-T. Janka, C. Pankow, and N. Stergioulas, *Phys. Rev. D* **90**, 062004 (2014).

[13] H. Yang, V. Paschalidis, K. Yagi, L. Lehner, F. Pretorius, and N. Yunes, *Phys. Rev. D* **97**, 024049 (2018).

[14] A. Torres-Rivas, K. Chatzioannou, A. Bauswein, and J. A. Clark, *Phys. Rev. D* **99**, 044014 (2019).

[15] J. M. Lattimer and M. Prakash, *Physics Reports* **621**, 127 (2016), memorial Volume in Honor of Gerald E. Brown.

[16] F. Özel and P. Freire, *Annual Review of Astronomy and Astrophysics* **54**, 401 (2016), <https://doi.org/10.1146/annurev-astro-081915-023322>.

[17] K. Yagi and N. Yunes, *Physics Reports* **681**, 1 (2017), approximate Universal Relations for Neutron Stars and Quark Stars.

[18] K. Yagi and N. Yunes, *Classical and Quantum Gravity* **33**, 13LT01 (2016).

[19] K. Yagi and N. Yunes, *Classical and Quantum Gravity* **34**, 015006 (2016).

[20] K. Yagi and N. Yunes, *Science* **341**, 365 (2013).

[21] K. Yagi and N. Yunes, *Phys. Rev. D* **88**, 023009 (2013).

[22] J. M. Lattimer and M. Prakash, *The Astrophysical Journal* **550**, 426 (2001).

[23] F. Özel and D. Psaltis, *Phys. Rev. D* **80**, 103003 (2009).

[24] J. M. Lattimer and A. W. Steiner, *The European Physical Journal A* **50**, 40 (2014).

[25] C. Drischler, J. Holt, and C. Wellenhofer, *Annual Review of Nuclear and Particle Science* **71**, null (2021), <https://doi.org/10.1146/annurev-nucl-102419-041903>.

[26] H. T. Cromartie, E. Fonseca, S. M. Ransom, P. B. Demorest, Z. Arzoumanian, H. Blumer, P. R. Brook, M. E. DeCesar, T. Dolch, J. A. Ellis, R. D. Ferdman, E. C. Ferrara, N. Garver-Daniels, P. A. Gentile, M. L. Jones, M. T. Lam, D. R. Lorimer, R. S. Lynch, M. A. McLaughlin, C. Ng, D. J. Nice, T. T. Pennucci, R. Spiewak, I. H. Stairs, K. Stovall, J. K. Swiggum, and W. W. Zhu, *Nature Astronomy* , 1 (2019).

[27] E. Fonseca, H. T. Cromartie, T. T. Pennucci, P. S. Ray, A. Y. Kirichenko, S. M. Ransom, P. B. Demorest, I. H. Stairs, Z. Arzoumanian, L. Guillemot, A. Parthasarathy, M. Kerr, I. Cognard, P. T. Baker, H. Blumer, P. R. Brook, M. DeCesar, T. Dolch, F. A. Dong, E. C. Ferrara, W. Fiore, N. Garver-Daniels, D. C. Good, R. Jennings, M. L. Jones, V. M. Kaspi, M. T. Lam, D. R. Lorimer, J. Luo, A. McEwen, J. W. McKee, M. A. McLaughlin, N. McMann, B. W. Meyers, A. Naidu, C. Ng, D. J. Nice, N. Pol, H. A. Radovan, B. Shapiro-Albert, C. M. Tan, S. P. Tendulkar, J. K. Swiggum, H. M. Wahl, and W. W. Zhu, *The Astrophysical Journal Letters* **915**, L12 (2021).

[28] A. M. Anile, *Relativistic Fluids and Magneto-fluids: With Applications in Astrophysics and Plasma Physics*, Cambridge Monographs on Mathematical Physics (Cambridge University Press, 1990).

[29] S. W. Hawking and G. F. R. Ellis, *The Large Scale Structure of Space-Time* (Cambridge University Press, 1973) p. 404.

[30] S. A. Bludman and M. A. Ruderman, *Phys. Rev.* **170**, 1176 (1968).

[31] S. A. Bludman and M. A. Ruderman, *Phys. Rev. D* **1**, 3243 (1970).

[32] S. Koranda, N. Stergioulas, and J. L. Friedman, *The Astrophysical Journal* **488**, 799 (1997).

[33] P. Bedaque and A. W. Steiner, *Phys. Rev. Lett.* **114**, 031103 (2015).

[34] D. M. Podkowka, R. F. P. Mendes, and E. Poisson, *Phys. Rev. D* **98**, 064057 (2018).

- [35] J. B. Hartle, *Astrophys. J.* **150**, 1005 (1967).
- [36] C. Breu and L. Rezzolla, *Monthly Notices of the Royal Astronomical Society* **459**, 646 (2016), <https://academic.oup.com/mnras/article-pdf/459/1/646/8113938/stw575.pdf>.
- [37] T. Hinderer, *Astrophys. J.* **677**, 1216 (2008).
- [38] T. Damour and A. Nagar, *Phys. Rev. D* **80**, 084035 (2009).
- [39] T. Binnington and E. Poisson, *Phys. Rev. D* **80**, 084018 (2009).
- [40] B. P. Abbott *et al.*, *Classical and Quantum Gravity* **37**, 045006 (2020).
- [41] M. F. O’Boyle, C. Markakis, N. Stergioulas, and J. S. Read, *Phys. Rev. D* **102**, 083027 (2020).
- [42] J. Read, B. Lackey, B. Owen, and J. L. Friedman, *Phys. Rev. D* **79**, 124032 (2009), 0812.2163.
- [43] B. Margalit and B. D. Metzger, *The Astrophysical Journal* **850**, L19 (2017).
- [44] L. Rezzolla, E. R. Most, and L. R. Weih, *The Astrophysical Journal* **852**, L25 (2018).
- [45] M. Ruiz, S. L. Shapiro, and A. Tsokaros, *Phys. Rev. D* **97**, 021501 (2018).